Mechanism of Trivalent Gold Reduction and Reactivity of Transient Divalent and Monovalent Gold Ions Studied by Gamma and Pulse Radiolysis

G. R. Dey,[†] A. K. El Omar,[‡] J. A. Jacob,[‡] M. Mostafavi,[‡] and J. Belloni*[,‡]

Radiation and Photochemistry Division, Bhabha Atomic Research Centre, Trombay, Mumbai 400085, India, and Laboratoire de Chimie Physique/ELYSE, UMR UPS-CNRS 8000, Bât. 349, Universite' Paris-Sud, 91405, Orsay, France

Received: October 8, 2010; Revised Manuscript Received: December 1, 2010

The detailed kinetics of the multistep mechanism of the Au^{III} ion reduction into gold clusters have been investigated by radiation chemistry methods in 2-propanol. In particular, a discussion on the steady state radiolysis dose-dependence of the yields concludes to a comproportionation reaction of nascent gold atoms Au^0 with excess Au^{III} ions into Au^{II} and Au^{I}. This reaction should be achieved through Au^{III} consumption before the coalescence of atoms Au^0 into gold clusters may occur. Then gold clusters catalyze the reduction of Au^{I} by 2-propanol. It was also found that a long-lived Au^{II} dimer, $(Au^{II})_2$, was transiently formed according to the quantitative analysis of time-resolved absorbance signals obtained by pulse radiolysis. Then the disproportionation of Au^{II} is intramolecular in the dimer instead of intermolecular, as usually reported. The yields, reaction rate constants, time-resolved spectra, and molar extinction coefficients are reported for the successive one-electron reduction steps, involving especially the transient species, such as Au^{II}, $(Au^{II})_2$, and Au^{I}. The processes are discussed in comparison with other solvents and other metal ions.

Introduction

Since a few decades, the specific properties of metal clusters and the mechanism of their formation are receiving increasing attention.[1] In this respect, radiation chemistry in the regime of pulse radiolysis or in the steady regime of γ-radiolysis is a particularly potent method to study oxidation and reduction processes and the properties of the short-lived and unusual metal valency states.[2] Series of metal clusters have been synthesized by the radiolytic method.[3,4] However, compared to the numerous studies on the reduction into atoms of monovalent ions, specially of silver in different aqueous and nonaqueous media,[4] the elucidation of the cluster production mechanism via the reduction of multivalent ions as precursors is generally faced to the difficulty of the overlapping of the optical absorption spectra of several transient valency states. Thus, very few time-resolved optical spectroscopy studies on the several steps of multivalent ion reduction are found in the literature.[4,5] In particular, despite gold clusters are specially studied, owing to their chemical stability and their newly discovered role in nonlinear optics,[6] catalysis[7] or medicine,[8] only one single work has been devoted to the time-resolved study of the trivalent gold ion reduction mechanism.[9] Baxendale and Koulkes-Pujo studied in water the reduction of trivalent gold ions in acidic solutions using pulse radiolysis.[9] Methanol was added as a scavenger of oxidizing radical $OH^{\bullet}$. Under these conditions the reduction of Au^{III} is achieved by $H^{\bullet}$ and methanol radicals. From time-resolved optical spectra data, the authors have derived the optical absorption spectrum of Au^{II}, which exhibits as for Au^{III} a high intensity below 250 nm. A specific shoulder is observed for Au^{II} at 275 nm with an extinction coefficient of 4.8×10^3 M^{-1} cm^{-1}. The isosbestic points for both Au^{III} and Au^{II} forms of gold ions in water are at 305 and 360 nm. It was found that Au^{II} then disappears by a second-order process that suggested a disproportionation reaction leading to Au^{I} and Au^{III}.[9]

A more recent γ-radiolysis study of Au^{III} reduction in water has shown that indeed the monovalent Au^{I} ions are rather stable and are not reduced by the radiolytic radicals unless Au^{III} are substantially consumed after the sample has absorbed a critical dose, so that an induction irradiation time is observed before the cluster formation.[10] Besides, 2-propanol is able to reduce very slowly Au^{I} adsorbed on clusters when these are radiolytically induced.

The present study aims to elucidate, using pulse and γ-radiolysis, the stepwise mechanism of the formation of the successive intermediate species during the reduction of Au^{III} ions into gold clusters. The solvent 2-propanol was chosen because, without any scavenger addition, both initial species radiolytically generated, namely e_{solv}^- and $(CH_3)_2C^{\bullet}OH$ (2-hydroxyl-2-propyl radical), display strong reducing properties. The radiolytic reduction of silver ions Ag^+,[11] copper ions Cu^{2+},[12] or iron ions Fe^{2+}[13] has been already studied in this solvent. Attempts are made here to derive at each step the kinetics, yields, and optical absorption spectra of the successive transient intermediates generated during the radiolysis in 2-propanol solutions of trivalent Au^{III} ion up to the gold clusters.

Experimental Section

Trivalent gold ions as $HAuCl_4$ trihydrate (99.9% purity) from Arora-Mathey Chemicals or Sigma-Aldrich, and $AuCl_3$ trihydrate (99.9% purity) from Alfa-Aora, 2-propanol (>99% purity) and methyl viologen chloride ($MVCl_2$) from Sisco Chemicals and Fluka, and polyethylene glycol (PEG MW = 42000) from Fluka were used as received. AnalaR grade Ar and N_2O gases from Indian Oxygen were used for purging the solutions.

The changes in the UV−vis spectra of 10^{-4} M Au^{III} ions recorded in water−2-propanol system with different component

* To whom correspondence should be addressed. E-mail: jacqueline.belloni@u-psud.fr.
[†] Bhabha Atomic Research Centre.
[‡] Laboratoire de Chimie Physique/ELYSE.

10.1021/jp1096597
Published on Web 12/21/2010

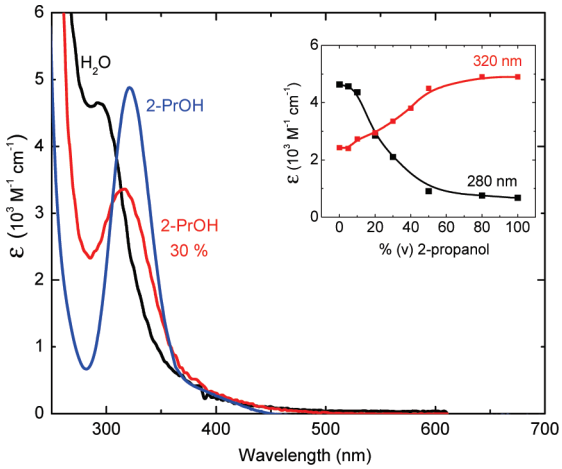

Figure 1. UV−vis spectra of $HAuCl_4$ solution in water, in 2-propanol, and in the mixed solvent at 30% v/v in 2-propanol. Inset: Absorbance at 320 nm vs % v/v of 2-propanol (0.1 mM $HAuCl_4$, optical path 10 mm).

ratios are shown in Figure 1. In neat 2-propanol, the maximum of the absorption band at 320 nm is red-shifted (compared to 290 nm in water)[9] and a minimum is observed at 280 nm (Figure 1 and Table 1 in SI). It is important to note here that, although 2-propanol is known as a mild reducing agent, it is unable to reduce Au^{III} ions directly. The solutions are stable indeed and the spectra unchanged as it was checked by keeping Au^{III} ions in different mixed solutions for a long time (>7 days).

The γ-radiolysis experiments on Au^{III} ion solutions in 2-propanol were carried out using the Co^{60} γ-source at BARC (dose rate 1.8 kGy h^{-1} = 1.8 kJ kg^{-1} h^{-1}) or at Laboratoire de Chimie Physique, Orsay (dose rate ≤ 2 kGy h^{-1} = 2 kJ kg^{-1} h^{-1}). The dose rate was measured using the Fricke dosimeter. The UV−vis spectra produced during the γ-radiolysis were recorded in a spectrophotometer HP Chem. 8453. Suprasil quartz cells having 2 or 10 mm optical path lengths were used for γ-irradiation for gold 2-propanolic solutions in presence and in absence of PEG.

Pulse radiolysis studies were carried out using 7 MeV electron pulses of 50 ns, 500 ns and 2 μs duration from a linear electron accelerator (Forward Industries, UK). The experimental set up for pulse radiolysis in BARC has been described earlier.[14] Aerated 0.01 M potassium thiocyanate aqueous solution was used as a dosimeter for determining the absorbed dose using a $G\epsilon$ value of 2.59 × 10^{-4} m^2 J^{-1} for the $(SCN)_2^{-\cdot}$ radical at 475 nm.[15] Doses per pulse in water used for the present study were 15, 40, and 112 Gy per pulse for 50 ns, 500 ns and 2 μs pulses, respectively. The corresponding doses in 2-propanol were calculated in J L^{-1} using the electronic density of the medium (for 2-propanol ρ = 0.785 kg L^{-1} and the electronic density ratio with respect to water is 0.799).[16] The doses in 2-propanol were therefore 12, 32, and 90 J L^{-1} per pulse, respectively. The optical path of the suprasil irradiation cell was 1 cm. During the experiments, the solutions were changed after each electron pulse.

The species generated during the radiolysis of deaerated 2-propanol through different reactions following the initial ionization and excitation of the solvent are, by analogy with other alcohols[17] or aqueous solutions of 2-propanol,[18,19] the following:

$$(CH_3)_2CHOH \rightsquigarrow (CH_3)_2CHOH^*, (CH_3)_2CHOH^{+\cdot}\ e^- \quad (1)$$

$$e^- + (CH_3)_2CHOH \rightarrow e^-_{solv} \quad (2)$$

$$(CH_3)_2CHOH^* \rightarrow H^\bullet + (CH_3)_2C^\bullet OH \quad (3)$$

Side reactions also occur in the radiolysis of neat 2-propanol, leading to other radicals and to final products, but their yields are of much less importance.[20]

According to the literature,[21] $H^\bullet$ atoms react with 2-propanol (reaction rate constant = 7.4 × 10^7 M^{-1} s^{-1} in aqueous system):[22]

$$H^\bullet + (CH_3)_2CHOH \rightarrow (CH_3)_2C^\bullet OH + H_2 \quad (4)$$

Simultaneously with α-hydroxypropyl radicals $(CH_3)_2C^\bullet OH$, alkoxy radicals $(CH_3)_2CHO^\bullet$ may be also formed but they are converted to the first form by rapid H-abstraction from α-position.

The primary cation $(CH_3)_2CHOH^+$ undergoes a reaction with the solvent molecules:

$$(CH_3)_2CHOH^{+\bullet} + (CH_3)_2CHOH \rightarrow (CH_3)_2CHOH_2^+ + (CH_3)_2C^\bullet OH \quad (5)$$

The transient optical spectrum obtained on pulse radiolysis of 2-propanol has an absorption maximum around 820 nm due to the formation of e_{solv}^-.[23] The molar absorption coefficient $\varepsilon_{820}(e_{solv}^-)$ is 1.3 × 10^4 M^{-1} cm^{-1}.[23] In the absence of any added solute, the solvated electron decays mostly by reaction

$$e^-_{solv} + (CH_3)_2CHOH_2^+ \rightarrow H^\bullet + (CH_3)_2CHOH \quad (6)$$

$H^\bullet$ atoms then react by eq 4. Solvated electrons decay also by reaction 7:

$$e^-_{solv} + e^-_{solv} \rightarrow H_2 + 2(CH_3)_2CHO^- \quad (7)$$

The reaction of e_{solv}^- with the radical $(CH_3)_2C^\bullet OH$ is much slower and negligible. The α-hydroxypropyl radicals decay by dimerization or disproportionation:

$$(CH_3)_2C^\bullet OH + (CH_3)_2C^\bullet OH \rightarrow (CH_3)_2(OH)CC(OH)(CH_3)_2 \quad (8)$$

$$(CH_3)_2C^\bullet OH + (CH_3)_2C^\bullet OH \rightarrow (CH_3)_2CO + (CH_3)_2CHOH \quad (8')$$

Solvated electrons e_{solv}^- are strong reducing agents which are able to reduce all metal ions. Due to 4, $H^\bullet$ atoms react directly with the solvent and not with the low concentration of metal ions present in alcohol. However, the $(CH_3)_2C^\bullet OH$ radicals originating from reactions 3−5 display also reducing properties (E° $(CH_3)_2CO + H^+ / (CH_3)_2C^\bullet OH$ = −1.4 V_{NHE} in neutral water)[24] and take an active part in metal ion reduction. In a N_2O purged system, e_{solv}^- also leads to α-hydroxypropyl radical via reactions 9 and 9′:

$$e^-_{solv} + N_2O \rightarrow N_2 + O^{\bullet -} \quad (9)$$

$$O^{\bullet -} + (CH_3)_2CHOH \rightarrow (CH_3)_2C^{\bullet}OH + OH^- \quad (9')$$

Alcohol radicals are then the only transient species interacting with metal ions for their reduction.

Results and Discussion

Steady-State Radiolysis. The γ-radiolysis experiments on Ar-purged 2-propanol solutions were carried out at different gold ion concentrations $[HAuCl_4] = (0.1 \text{ to } 1) \times 10^{-3}$ M. The band intensity at the maximum wavelength 320 nm of the initial unirradiated solution corresponds to a molar absorption coefficient of $\epsilon_{320}(Au^{III}) = 4880 \pm 50$ M^{-1} cm^{-1}. The UV−vis spectra recorded at increasing dose for irradiated samples at $[HAuCl_4] = 5 \times 10^{-4}$ M are shown in Figure 2a. The band intensity at 320 nm decreases linearly up to a complete bleaching at 1.7 kJ L^{-1} (Figure 2b). Within this dose range, no absorption is observed beyond 450 nm, and at any dose the band positions of the maximum at 320 nm and minimum at 280 nm are unchanged. Immediately beyond 1.7 kJ L^{-1}, the sample acquires progressively a pale purple color and the spectrum exhibits the specific surface plasmon absorption band having a maximum at around 560 nm and an additional new increasing intensity in the UV region (Figure 2a). However, the visible band is very broad and even at the highest dose of the plateau (4 kJ L^{-1}, Figure 2b) the intensity is low. The molar absorption coefficient is only $\varepsilon_{560}(Au_n) \approx 800$ M^{-1} cm^{-1} (compared to 3200 M^{-1} cm^{-1} in water in the presence of PVA),[10] meaning that the gold particles are very large. Same results were obtained with the salt $AuCl_3$ at 2×10^{-4} M (Figure 2c), except that at this concentration the complete bleaching is now observed at a smaller dose (0.65 kJ L^{-1}), and the plateau of zerovalent gold corresponds to a molar absorption coefficient close to 1400 M^{-1} cm^{-1}.

To get better accuracy on the formation of gold clusters, the dose-dependent absorbance was measured in the presence of PEG 5×10^{-2} M (initial concentration $[Au^{III}] = 2 \times 10^{-4}$ M). The decay of the Au^{III} absorbance is also linear with the same slope as without PEG. However, despite the presence of PEG, the 560 nm band is surprisingly as broad and weakly intense as without polymer. The distribution of the particle sizes, observed by DLS, ranges from 5 to 100 nm with a maximum at 50 nm. It seems that the binding of PEG with gold clusters in 2-propanol is too weak to prevent their approach and coalecence.

It is remarkable that in both cases the appearance of clusters at 560 nm is delayed to a critical dose (1.7 kJ L^{-1} for $[Au^{III}] = 5 \times 10^{-4}$ M; Figure 2b). At the end of this induction period, the Au^{III} ions have just completely disappeared and Au^I is therefore the only stable product present. Its formation rate is thus equal to the Au^{III} disappearance rate. It is clear that if the spectrum at the end of the induction period of 1.7 kJ L^{-1} is assigned to Au^I, its absorbance in the range 260−700 nm is negligible (Figure 2a).

Because the tetrachloro auric acid $HAuCl_4$ contains a proton, protonated alcohol $(CH_3)_2CHOH_2^+$ is formed and can react with solvated electrons (reaction 6). At increasing dose, the concentration of H^+ also increases as a product of the reduction 11, and favors reaction 6. Then $H^{\bullet}$ atoms produce $(CH_3)_2C^{\bullet}OH$ radicals via reaction 4. In this low-polarity solvent, the rate constant of reaction 6 between opposite charged species is certainly faster than that of e_{solv}^- with $AuCl_4^-$. The initial steps of reduction of $AuCl_4^-$ ions are thus essentially achieved by alcohol radicals $R^{\bullet}$ and, only at a small extent, by solvated electrons, while the positive gold ions in $AuCl_3$ solutions are reduced by both:

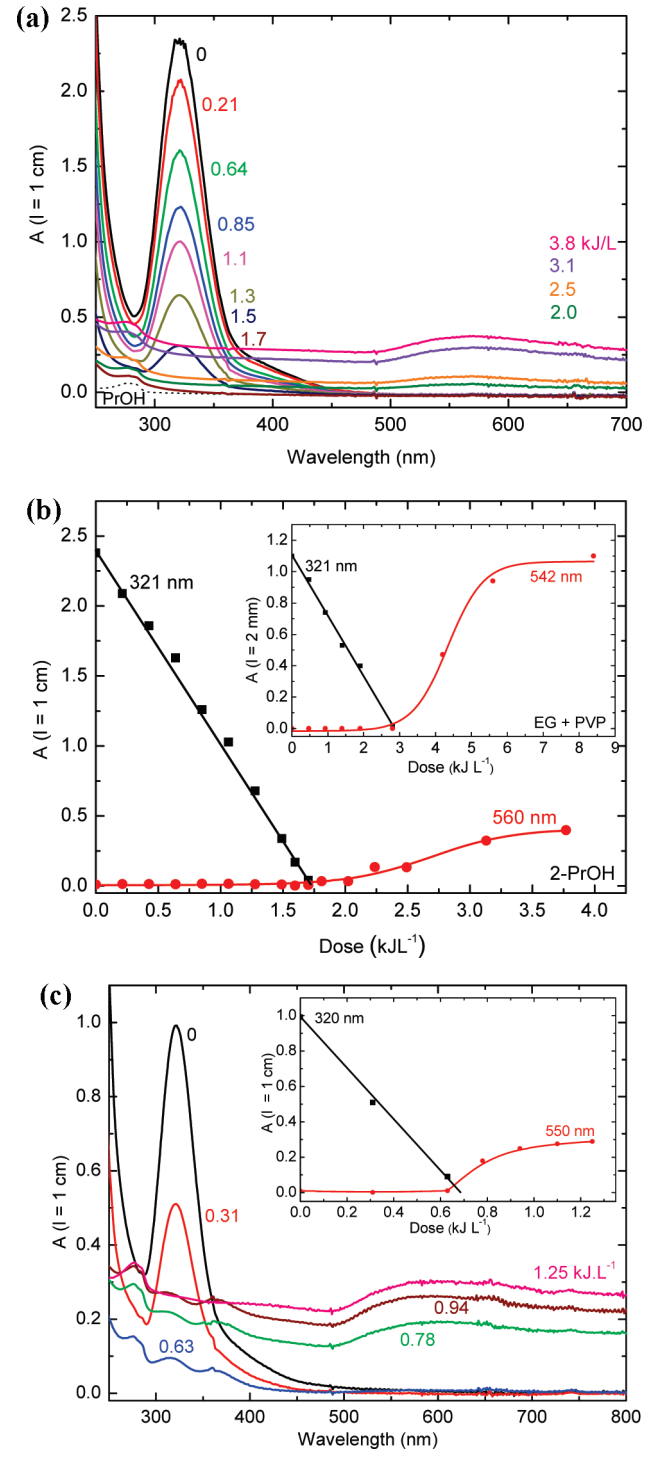

Figure 2. (a) Optical absorption spectra during the γ-radiolysis of $HAuCl_4$ at 5×10^{-4} M in 2-propanol. Labels are in kJ L^{-1}. Neat 2-propanol spectrum is shown for comparison (optical path: 1 cm; reference: water). (b) Variation wih dose of the absorbance at 321 and 560 nm. Inset: Absorbance variation versus the dose of $AuCl_4^-$ at 321 nm and of Au clusters at 542 nm in ethylene glycol solutions of $HAuCl_4$ at 10^{-3} M containing 0.1 M PVP. Data taken from ref 30. (c) Optical absorption spectra during the γ-radiolysis of $AuCl_3$ at 2×10^{-4} M in 2-propanol with 0.5 M PEG. Labels are in kJ L^{-1} (optical path: 1 cm; reference: water). Inset: Variation wih dose of the absorbance at 321 and 560 nm.

$$Au^{III} + e^-_{solv} \rightarrow Au^{II} \quad (10)$$

$$Au^{III} + R^\bullet \rightarrow Au^{III}R^\bullet \rightarrow Au^{II} + (CH_3)_2CO + H^+ \quad (11)$$

The transient complexation with $R^\bullet$ before reduction has been observed in aqueous solutions of Ag^+ containing 2-propanol[25] and is tentatively supposed also in 2-propanol solvent. Acetone is produced by (11) and is known to also scavenge efficiently e^-_{solv}, but the radical anion $(CH_3)_2CO^{-\bullet}$ then reduces eventually Au^{III}.

The same symbol, Au^{II}, is used for all bivalent ions, more or less complexed by Cl^- or not. The Au^{II} species are known to be unstable. From pulse radiolysis data in water,[9] they were supposed to disproportionate:

$$Au^{II} + Au^{II} \rightarrow Au^{III} + Au^{I} \quad (12)$$

From the linear decrease of the absorbance at 320 nm (Figure 2b and Figure 3) and the molar absorption coefficient $\varepsilon_{320}(Au^{III})$, we derive the yield $G(-Au^{III})$, which is the same for $HAuCl_4$ or $AuCl_3$, with or without PEG:

$$G(-Au^{III}) = G(Au^{I}) = 2.9 \times 10^{-7} \text{mol J}^{-1}$$

The two-electron reduction yield G_{red} of Au^{III} into Au^{I} is:

$$G_{red}=2G(-Au^{III}) = 2G(Au^{I}) = G(e_s^-) + G(R^\bullet) = 5.8 \times 10^{-7} \text{mol J}^{-1}$$

It is probable that during its accumulation, Au^{I} may progressively compete with Au^{III} and react with the reducing radicals, after complexation with the radical, as shown for Ag^+:[25,26]

$$Au^{I} + e^-_{solv} \rightarrow Au^{0} \quad (13)$$

$$Au^{I} + R^\bullet \rightarrow Au^{I}R^\bullet \rightarrow Au^{0} + (CH_3)_2CO + H^+ \quad (14)$$

Then, the association of gold atoms with excess Au^{I} ions is followed by their coalescence into gold clusters, the overall process being:

$$nAu^0 \rightarrow Au_n \quad (15)$$

However, according to the results and in contrast with this hypothesis, no reduction product of Au^{I}, such as Au_n, issued from reactions 13−15 is observed during the induction time as far as Au^{III} is still present.

One possible reason could be that in 2-propanol the competitive reduction reactions 13 and 14 of Au^{I} are much slower than those of Au^{III} reactions 9′ and 11, but this is in contradiction at least with the high reduction rate constant of monovalent Au^{I}, in the form of the cyano-complex, as measured by pulse radiolysis in water, $k(AuCN_2^- + e_{aq}^-) = 3.5 \times 10^9 \text{ M}^{-1} \text{ s}^{-1}$.[27,28] Another possibility is a higher complexation constant with the radical for the reaction of Au^{III} than of Au^{I}, thus, favoring the reduction of Au^{III}:

$$Au^{I}R^\bullet + Au^{III} \rightarrow Au^{I} + Au^{III}R^\bullet \quad (16)$$

When the nascent gold atoms Au^0 are produced in reactions 13 and 14, they also may be readily consumed via a process distinct from coalescence (15). Actually, the reduction potential of the isolated atom is very negative, the difference with the reduction potential value for bulk gold metal being equal to the sublimation energy of the metal[29] ($\Delta H_{sub} = 3.66$ eV, so that in water $E^o(Au^+/Au^0)_{Cl-} = -2.5$ V_{NHE} instead of $E^o(Au^+/Au_{metal})_{Cl-} = +1.15$ V_{NHE}). Hence, the newly formed atoms Au^0 would be able to reduce readily the Au^{III} ions into Au^{II} as far as Au^{III} is still present in the solution (a reaction of Au^0 with Au^{II} is unlikely because the steady state concentration of Au^{II} is much lower than that of Au^{III}). The proposed mechanism is actually the comproportionation reaction 17:

$$Au^{0} + Au^{III} \rightarrow Au^{I} + Au^{II} \quad (17)$$

As a result of reaction 16 or 17, Au^{III} is stoichiometrically converted into Au^{I} as the only stable irradiation product, directly by the radiolytic species or indirectly through the transient formation of Au^0, as far as Au^{III} is not totally consumed, thus, preventing the appearance of zerovalent gold during an induction time. At the dose of 1.7 kJ L^{-1}, the weakly intense absorption spectrum in Figure 2a is that of Au^{I} at 5×10^{-4} M (Table 1 in SI). The solutions of Au^{I} are stable because no absorbance change is observed on aging or in presence of air. The ions Au^{I} are not reduced by the solvent into Au_n or oxidized by oxygen into Au^{III}. Moreover, a spontaneous disproportionation of $2Au^{I}$ into Au^0 and Au^{II} is thermodynamically ruled out, due to the high negative reduction potential of $E^o(Au^{I}/Au^0)_{Cl-}$. In fact, the reduction potential $E^o(Au^{I}/Au^0)_{Cl-}$ is much lower than $E^o(Au^{II}/Au^{I})_{Cl-}$ and not higher as required for a disproportionation.

Note that a similar induction time prior the gold clusters formation was observed in water[10,30] and also recently in ethylene glycol,[31] without being explained. The absorbance of Au^{III} in ethylene glycol (initially $[Au^{III}] = 10^{-3}$ M) was also found to decay linearly with the dose up to the total bleaching of Au^{III} at 2.8 kJ L^{-1} without any formation of gold clusters as well (Figure 2b, inset). The reduction yield of Au^{III} in ethylene glycol is $G_{EG}(-Au^{III}) = G_{EG}(Au^{I}) = 3.4 \times 10^{-7}$ mol J^{-1}, that is slightly higher than in 2-propanol ($G_{2\text{-PrOH}}(-Au^{III}) = 2.9 \times 10^{-7}$ mol J^{-1}). At that critical dose, the only stable species is Au^{I}, which does not absorb in the range 250−700 nm. Then, at increasing dose, the formation of clusters starts. This peculiar feature of the delayed formation of Au_n can be accounted for in ethylene glycol[30] or water[10,30] by the same reaction 17 of comproportionation as in 2-propanol.

Another example of delayed formation of clusters was observed in 2-propanolic solutions of Cu^{2+}.[12] At the concentration of 1.5×10^{-4} M, an induction dose of 0.24 kJ L^{-1} is required before the surface plasmon band of Cu_n is observed. On average, the one-electron reduction yield of Cu^{2+} into Cu^+ is $G_{red} = 6.2 \times 10^{-7}$ mol J^{-1}, in good agreement with gold solutions. The delayed formation of copper clusters observed by the author[12] also means that, according to the above mechanism, Cu^0 atoms, competitively produced by Cu^+ ions, are able to reduce Cu^{2+} because the reduction potential value is very negative, $E°(Cu^+/Cu^0) = -2.4$ V_{NHE}[4], as is $E°(Au^{I}/Au^0)$. Hence, Cu^0 or Cu_n are not observed as far as Cu^{2+} are still present, as in the case of Au^0 and Au^{III} in reaction 17.

At high dose, after the complete reduction of Au^{III} into Au^{I}, Au^0 atoms are formed by the radiolytic reduction of Au^{I} and

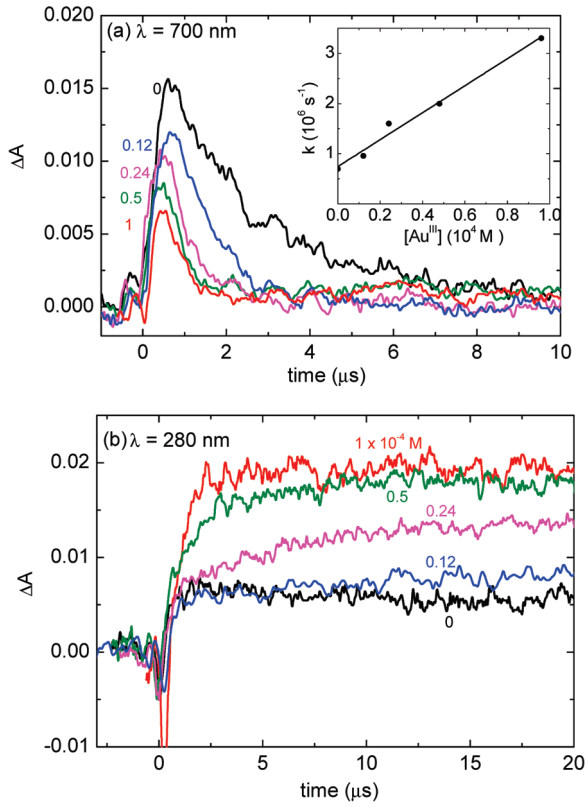

Figure 3. (a) Time profiles of the differential absorbance at 700 nm after the electron pulse in Ar-purged 2-propanol containing different concentrations of $AuCl_4^-$ ions (dose per pulse = 12 J L^{-1}). Labels are in 10^{-4} M of Au^{III}. Optical path: 10 mm. Inset: Plot of pseudo-first-order rate constant vs [Au^{III}]. (b) Time profiles of the differential absorbance at 280 nm after electron pulse irradiation of Ar-purged 2-propanol containing different concentrations of $AuCl_4^-$ ions. Labels are in 10^{-4} M of Au^{III}. Optical path: 1 cm.

coalesce into clusters Au_n (reactions 13−15). In 2-propanol, the absorbance increase at 560 nm up to the plateau is achieved at a total dose of 3.7 J L^{-1} (Figure 2b). As soon as formed, the atoms coalesce via reaction 15 or associate with Au^I and the clusters adsorb Au^I ions, which are reduced by radiolytic species in situ:

$$Au^I + Au_n \rightarrow Au^I Au_n \quad (18)$$

$$Au^I Au_n + e^-_{solv} \rightarrow Au_{n+1} \quad (19)$$

$$Au^I Au_n + (CH_3)_2C^{\bullet}OH \rightarrow Au_{n+1} + (CH_3)_2CO + H^+ \quad (19')$$

The polymer PEG does not prevent the coalescence (14) and the final size of clusters is large, while in ethylene glycol with PVP (Figure 2b, inset) the intense and narrow plasmon band ($\varepsilon_{550}(Au_n)_{EG} \approx 5500$ M^{-1} cm^{-1}) indicates that small clusters (10−15 nm, measured by TEM) are stabilized by PVP.

From the slope of the reduction curve of Au^I into gold clusters (5×10^{-4} M Au^I are reduced within about 1.7 kJ L^{-1}), the yield is equal to only $G(-Au^I) = 3 \times 10^{-7}$ mol J^{-1}, that is, about $G_{red}/2$ in 2-propanol (Figure 2b,c) as well as in ethylene glycol (Figure 2b, inset), and not to G_{red} as expected. The radiolytic radicals are thus only partially scavenged by Au^I and undergo other processes than the reduction reactions (14 and 19′). They may disappear by dimerization, disproportionation, or a reaction catalyzed by the gold clusters, producing molecular hydrogen. Indeed, such a reaction has been demonstrated to occur in presence of several metal clusters.[32] However, that implies that, to be efficient, these second-order processes have comparable rates with the monovalent gold reduction into Au^0 which is expected to be not thermodynamically favored. The same remarks are valid for the gold reduction in ethylene glycol.

Pulse Radiolysis. Note first that the doses per pulse are in the range of 12 to 90 J L^{-1}, which is much less than the doses previously absorbed in γ-radiolysis. Hence, just after the pulse, the concentration of the radiolytic species is now very small compared to the initial solute Au^{III} concentration. The reducing species are totally scavenged by Au^{III} and only a small fraction of Au^{III} is reduced into a lower valency.

Scavenging Rate Constants of Au^{III} in 2-Propanol. The decay of e_{solv}^- in neat Ar-purged 2-propanol and the reaction kinetics of e_{solv}^- with Au^{III} ion (reaction 9′) were studied in $HAuCl_4$ 2-propanolic solutions in the range $(0.12 - 1) \times 10^{-4}$ M after a pulse of 50 ns and 12 J L^{-1} (Figure 3a). At 700 nm, corresponding to the absorption band of e_{solv}^- ($\lambda_{max} = 820$ nm),[23] the absorbance at the end of the pulse in neat solvent is $A = 0.015$. Accounting for the molar absorption coefficient at 700 nm $\varepsilon_{700}(e_{solv}^-) = 1.1 \times 10^4$ M^{-1} cm^{-1},[33] the initial concentration is $[e_{solv}^-]_{500\ ns} = 1.36 \times 10^{-6}$ M and the yield of the solvated electron is $G(e_{solv}^-)_{500\ ns} = 1.12 \times 10^{-7}$ mol J^{-1}. The initial absorbance of e_{solv}^- decreases when [$HAuCl_4$] increases, meaning that e_{solv}^- are also scavenged during the pulse and that the yield of solvated electrons scavenged by $HAuCl_4$ is somewhat higher than in neat solvent and close to the literature value at ns range ($G(e_{solv}^-)_{ns} = 1.3 \times 10^{-7}$ mol J^{-1}).[34] The decay of the e_{solv}^- absorbance obeys a pseudofirst order. The rate of the e_{solv}^- decay at 700 nm increases linearly with [$HAuCl_4$] (Figure 3a, inset). The reaction rate constant, as determined from the slope of the pseudofirst order rate constant plot versus [$HAuCl_4$] is $k = 2.6 \times 10^{10}$ M^{-1} s^{-1}. As discussed above, the solvated electrons e_{solv}^- are more probably scavenged by the protons H^+ reaction 6. The $H^{\bullet}$ atoms produced react with the alcohol (reaction 4) giving the radicals $R^{\bullet}$, which then reduce Au^{III} into Au^{II} (reaction 11).

Under the same conditions as in Figure 3a, Figure 3b presents the corresponding increase at 280 nm of the differential absorbance with respect to the initial absorbance $[Au^{III}]_{280}$ before the pulse. The absorbance build-up at 280 nm, which is observed in the absence of gold ions is assigned to the α-hydroxy-propyl radicals. Their optical spectrum in water[21] or in neat 2-propanol[21a] is known to be a UV band extending to 350 nm and with a maximum below 220 nm. Moreover, the assignment is supported by the proportionality of the absorbances $A_{280\ nm}$ to the dose as reported in Figure 3b and in ref 21a.

In the presence of gold ions, the increase of the differential absorbance ΔA at 280 nm (within 2.5 μs at 10^{-4} M) is assigned to the replacement of Au^{III}, which also absorbs at 280 nm, by Au^{II} via the radical scavenging reaction 11. The differential absorbance at the plateau increases with [Au^{III}].

In order to determine the rate constant k_{11}, the pulse radiolysis was studied in N_2O-purged 2-propanol solutions, where e_{solv}^- is replaced by alcohol radicals reactions 8 and 9. Because the radical is not directly observable, k_{11} was determined, adopting the method of kinetics competition between Au^{III} and MV^{2+}, using the latter as a reference solute in N_2O-saturated solutions. The absorbance at 605 nm was monitored for the formation of $MV^{+\bullet}$. First, the rate constant of the radical scavenging by MV^{2+} is determined without Au^{III} at different concentrations of MV^{2+}

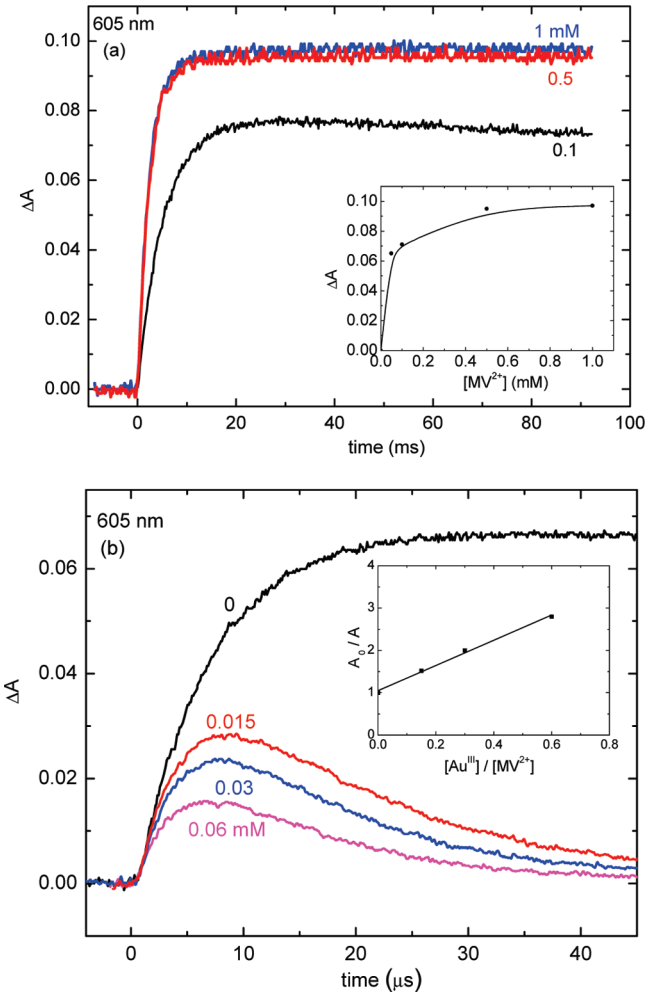

Figure 4. (a) Time profiles of the differential absorbance of $MV^{\bullet+}$ at 605 nm after electron pulse irradiation in N_2O-purged 2-propanol solutions of MV^{2+} at various concentrations (dose per pulse =12 J L^{-1}). Labels are in mM of MV^{2+}. Inset: Dependence of the differential absorbance of $MV^{\bullet+}$ at the plateau, ΔA_{max}, on the MV^{2+} concentration. (b) Time profiles of the differential absorbance of $MV^{\bullet+}$ at 605 nm after electron pulse irradiation in N_2O-purged 2-propanol solutions of MV^{2+} at 0.1 mM and at various concentrations of $HAuCl_4$. Labels are in mM of Au^{III}. Dotted line: bleached absorption spectrum calculated from the disproportionation of $2Au^{II}$ into Au^{III} and Au^{I}. Inset: Plot of A_0/A vs $[Au^{III}]/[MV^{2+}]$, where A_0 and A represent the absorbance values at 605 nm in N_2O-purged 2-propanolic solutions of $MV^{\bullet+}$ at 0.1 mM without and with different concentrations of Au^{III}, respectively.

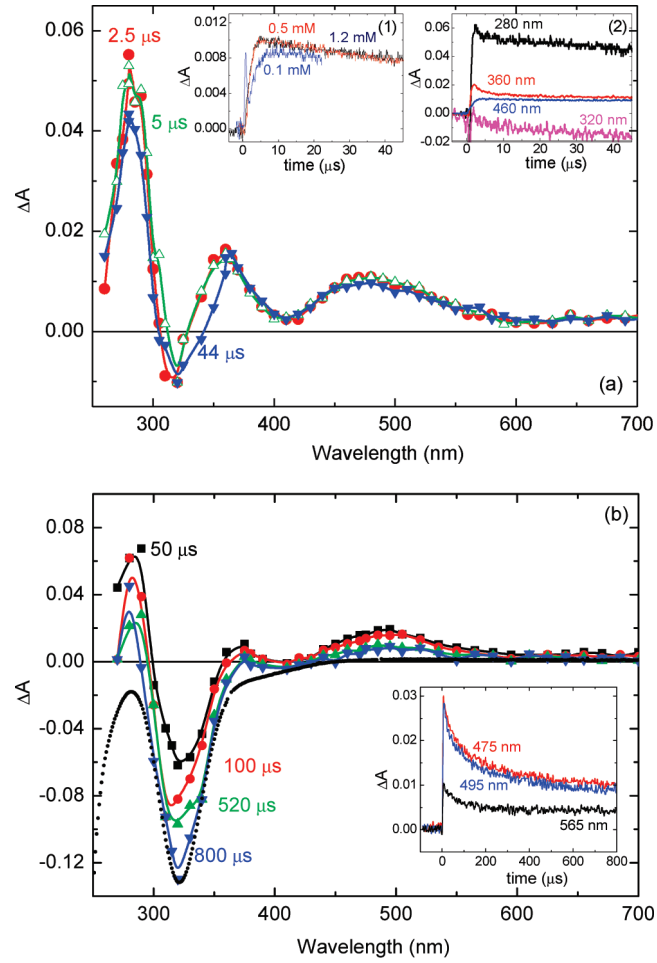

Figure 5. (a) Time-resolved transient absorption spectra obtained in electron pulse irradiated Ar-purged 5×10^{-4} M $HAuCl_4$ in 2-propanol after (-●-) 2.5, (-Δ-) 5, and (-▼-) 44 μs. Inset: (1) Time profiles obtained at 480 nm for different concentrations of Au^{III} ions; (2) Time profiles obtained at 280, 320, 380, and 480 nm in 0.5 mM Au^{III} solutions (dose per pulse = 32 J L^{-1}). (b) Time-resolved transient absorption spectra obtained in electron pulse irradiated Ar-purged 5×10^{-4} M $HAuCl_4$ 2-propanol solution after (-■-) 50, (-●-) 100, (-▲-) 520, and (-▼-) 800 μs. Dotted line: bleached absorption spectrum according to disproportionation of $2Au^{II}$ into Au^{III} and Au^{I}. Inset: time profiles obtained at 475, 495 and 565 nm (dose per pulse = 90 J L^{-1}).

ions (10^{-4} to 10^{-3} M; Figure 4a), as $k((CH_3)_2C^{\bullet}OH + MV^{2+}) = 1.5 \times 10^9$ M^{-1} s^{-1} (Figure 4a, inset; instead of 2.6×10^9 M^{-1} s^{-1} in water).[35] The total yield G_{red} of radiolytic reducing species in 2-propanol can be determined from the final absorbance of $MV^{+\bullet}$ at the plateau for 10^{-3} M and from the molar extinction coefficient, taken the same as in water: $\varepsilon_{605}(MV^{+\bullet}) = 1.37 \times 10^4$ M^{-1} cm^{-1}.[36] The total reduction yield is found to be $G_{red} = G(e_{solv}^-) + G(R^{\bullet}) = 6 \times 10^{-7}$ mol J^{-1}, close to the value given above by γ-radiolysis. Because $G(e_{solv}^-) = 1.3 \times 10^{-7}$ mol J^{-1}, the radical yield is $G(R^{\bullet}) = 4.7 \times 10^{-7}$ mol J^{-1}.

In the presence of the competitive reaction between Au^{III} and MV^{2+}, the $MV^{+\bullet}$ absorbance increase is slower, then it decays after around 10 μs, suggesting a further slow electron transfer from $MV^{+\bullet}$ to Au^{III} (Figure 4b). The inset presents the graph of the ratios of $MV^{+\bullet}$ absorbance without and with Au^{III} (or of the initial rates of $MV^{+\bullet}$ build-up) versus the $[Au^{III}]/[MV^{2+}]$ ratio. From the slope of the straight line in Figure 4b, inset and from the scavenging rate constant $k(R^{\bullet} + MV^{2+}) = 1.5 \times 10^9$ M^{-1} s^{-1}, the scavenging rate constant with Au^{III} in 2-propanol is found as $k_{11} = 7.6 \times 10^9$ M^{-1} s^{-1}.

Au^{II} Absorption Spectrum. The transient differential spectra with respect to the initial Au^{III} spectrum are shown in Figure 5a in the range 2.5 to 45 μs after a 500 ns pulse (dose per pulse of 32 J L^{-1}). The same time evolution of the spectrum is found in N_2O-saturated solutions. According to the kinetics signals at $[Au^{III}] = 5 \times 10^{-4}$ M in Figure 3b, all e_{solv}^- and radicals have been consumed within 2.5 μs. The $\Delta A_{2.5\mu s,280nm}$ values at 280 nm and at 2.5 μs after the pulse in Figure 3b and Figure 5a are proportional to the dose per pulse (with the ratio 32/12). From the reducing radical yield $G_{red} = 6 \times 10^{-7}$ mol J^{-1} as found above and the dose 32 J L^{-1}, the concentration of scavenged reducing species in Figure 5a is 1.9×10^{-5} M.

According to the kinetics in Figure 5a, the differential spectrum at 2.5 μs is hence assigned to the formation of $[Au^{II}] = 1.9 \times 10^{-5}$ M from Au^{III} reduction via reactions 9′ and 11. An identical spectrum was found at 1.2×10^{-3} M Au^{III} and decays within 800 μs (a long lifetime of a transient $Au^{III}R$ instead of Au^{II} is unlikely). The build-up rate of $\Delta A_{480\ nm}$ at 480 nm increases with initial $[Au^{III}]$ (Figure 5a, inset 1). Note

that, for 10^{-4} M $HAuCl_4$, an increase and a decay, both very fast, precede a subsequent slower increase assigned to the Au^{II} formation. The short-lived absorbance is due to e_{solv}^-, which also absorbs at 480 nm ($\varepsilon_{480}(e_{solv}^-) = 5000\ M^{-1}\ cm^{-1}$)[23] and which reacts faster than the formation of Au^{II} by the radicals reaction 11.

The first important feature of the differential spectrum at 2.5 μs in Figure 5a is that three positive bands appear ($\varepsilon Au^{II} > \varepsilon Au^{III}$) around the maxima 280, 360, and 480 nm. The second feature is that isosbestic points are observed at the wavelengths 250, 300, 325, and 410 nm between Au^{III} and Au^{II} ($\Delta A = 0$ and $\varepsilon Au^{II} = \varepsilon Au^{III}$). Finally, a slight bleaching is observed within 300 and 325 nm or in this range εAu^{II} is slightly lower than εAu^{III}.

The values of $\varepsilon_\lambda Au^{II}$ at different wavelengths may be calculated from ΔA by eq 20, with the value $[Au^{II}]_{2.5\ \mu s} = 1.9 \times 10^{-5}$ M, and from those of $\varepsilon_\lambda Au^{III}$, as given in Figure 1:

$$\Delta A_\lambda(\text{per cm}) = A_\lambda(Au^{II}) - A_\lambda(Au^{III}) = (\varepsilon_\lambda Au^{II} - \varepsilon_\lambda Au^{III}) \times [Au^{II}]_{2.5\mu s} \quad (20)$$

The values of $\varepsilon_\lambda Au^{II}$ so obtained for the Au^{II} spectrum are given in Table 1 (SI). It differs from Au^{III} spectrum essentially by a minimum, which is shifted from 280 to 300 nm with a higher intensity, between two maxima at 280 and 330 nm, and by a supplementary broad band of low intensity around 480 nm. The molar extinction coefficients at the maxima are $\varepsilon_{280nm}(Au^{II}) = 3300\ M^{-1}\ cm^{-1}$, $\varepsilon_{330nm}(Au^{II}) = 4760\ M^{-1}\ cm^{-1}$, and $\varepsilon_{480nm}(Au^{II}) = 530\ M^{-1}\ cm^{-1}$, respectively. For comparison, in water, the published absorption spectrum of Au^{II} has exibited a shoulder peaking at shorter wavelength, around 280 nm, but the domain above 380 nm was not studied.[9]

Au^{II} Reactivity. After the fast initial formation of Au^{II} up to 2.5 μs, the time profile curves at 280, 360, and 480 nm present a slow decay (Figure 5a, inset 2). Simultaneously, the bleaching at 320 nm also increases. Same features of a very slow decay are observed for the same solutions after a more intense pulse (dose per pulse 90 J L^{-1}; Figure 5b). The initial concentration of the radiolytic reducing species is now 5.4×10^{-5} M. The kinetics signals are also more intense than in Figure 5a, initially in the same ratio as the doses per pulse. A plateau is reached at around 800 μs (Figure 5b, inset).

It is generally accepted in the literature[9] that the decay of Au^{II} ions is due to a second-order disproportionation reaction and that the products are Au^{I} and Au^{III} because the overall material balance in γ-radiolysis corresponds to reaction 12. However, a thorough quantitative analysis based on the time-resolved spectra in 2-propanol within 2.5−800 μs does not support the hypothesis of a direct stoichiometrical replacement of $2Au^{II}$ by Au^{III} and Au^{I}. Although Au^{II} is the only reactive species, several arguments suggest excluding the hypothesis of the disproportionation (12):

(i) The spectrum at 800 μs does not correspond to the bleached absorption spectrum, as expected from the disproportionation and presented as the dotted spectrum in Figure 5b ($\Delta A_{bleach,\lambda} = 1/2(\varepsilon_\lambda Au^{III} - \varepsilon_\lambda Au^{I}) \times 5.4 \times 10^{-5}$ M). Note that, according to the γ-radiolysis results (Figure 2a), $\varepsilon_\lambda Au^{I} = 0$. In fact, the experimental differential spectrum still displays at 800 μs clearly positive bands at 280, 360, and 475 nm, which do not belong to Au^{III} nor Au^{I}. If the disproportionation (12) would occur, at least it could not be considered as achieved at 800 μs.

(ii) On the other hand, if we assume that the end differential spectrum corresponding to the bleaching $\Delta A_{bleach,\lambda}$ (dotted spectrum in Figure 5b according to reaction 12) would be reached at times much longer than 800 μs, and if we process the kinetics signals in a second-order plot as $1/(\Delta A_{t,\lambda} - \Delta A_{bleach,\lambda})$ versus time, we do not find straight lines.

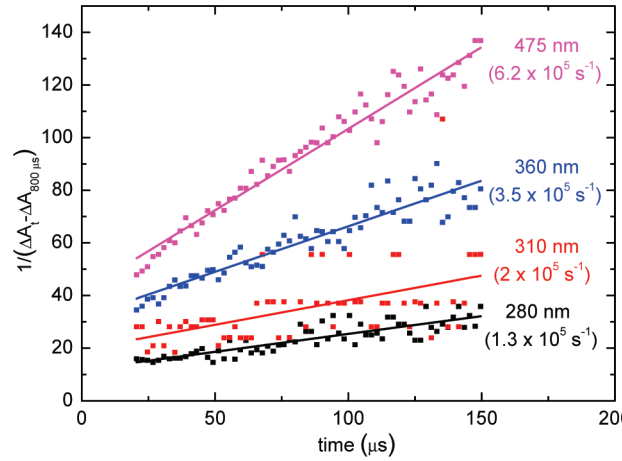

Figure 6. Plot of $1/(\Delta A_t - \Delta A_{800\mu s})$ vs time at 280, 310, 360, and 475 nm. Dose per pulse = 90 J L^{-1}. Values refer to $2k/l\varepsilon_\lambda$.

Therefore, to account for the results, we propose that the decay of Au^{II} is indeed a two-step process, the first one within 2.5−800 μs and the second one beyond 800 μs, which is too slow to be observed using our facility. Actually, the second-order plots versus time of the first step $1/(\Delta A_t - \Delta A_{800\mu s})$ gives now straight lines at 280, 310, 360, and 475 nm (Figure 6). That means that the differential spectrum at 800 μs should be thus assigned to a new transient species produced by a bimolecular reaction of Au^{II}, but distinct from reaction 12 and not producing $Au^{III} + Au^{I}$. The best candidate that could be alternatively issued from a second-order process is the intermediate transient dimer $(Au^{II})_2$ (reaction 21a):

$$Au^{II} + Au^{II} \xrightarrow{a} (Au^{II})_2 \xrightarrow{b} Au^{III} + Au^{I} \quad (21)$$

At longer time, the dimer $(Au^{II})_2$ would eventually undergo an internal electron transfer and first-order dissociation to produce Au^{III} and Au^{I} reaction (21b). This two-step process accounts quantitatively well for the features of the time-resolved signals observed until 800 μs. Besides, the overall material balance of the two-step dimerization-dissociation reaction 21 is equivalent to that of the disproportionation reaction 21 which was previously postulated[9] and supported by γ-radiolysis results. From the values of ΔA_{800}, we can obtain the molar absorption coefficient per atom of the dimer $\varepsilon_{at}(Au^{II})_2$ and hence the absorption spectrum of $(Au^{II})_2$ (Table 1 in SI), which will be presented further with the spectra of other gold species.

$$\Delta A_{800\mu s}(\text{per cm}) = A(Au^{II})_2 - A(Au^{III}) = (\varepsilon_{at}(Au^{II})_2 - \varepsilon Au^{III}) \times [Au^{II}]_{2.5\mu s} \quad (22)$$

In the whole domain, the maxima at 330 and 480 nm and the minimum at 300 nm are at the same wavelengths as for Au^{II}. However, the absorptivity per atom of the dimer $(Au^{II})_2$ is much less than for the monomer Au^{II}.

The slopes of the straight lines of the second-order plot in Figure 6 correspond to the ratio $2k_{21a}/[l \times (\varepsilon_{at}(Au^{II})_2 - \varepsilon Au^{II})]$. From the values of $\varepsilon_{at}(Au^{II})_2$ and Au^{II} (Table 1, SI) and from

the slopes at the various wavelengths in Figure 6, an average value is obtained for the dimerization rate constant $2k_{21a} = (2.9 \pm 0.6) \times 10^8$ M^{-1} s^{-1}. The value is independent of the wavelength in the range of uncertainties, thus confirming that only one single process occurs within 2.5 and 800 μs. The process is also dose-dependent as expected for a second-order reaction. Actually, when the data at 32 J L^{-1} per pulse are plotted at 310, 360, and 475 nm as in Figure 6, we obtain again straight lines. They have almost three times larger initial ordinates than in Figure 6, because the absorbances are three times lower. However, they are fairly parallel to the corresponding straight lines at 90 J L^{-1}, so confirming the rate constant.

The very slow second step of the $(Au^{II})_2$ decay, which is supposed to occur beyond 800 μs (reaction 21b) is not directly observed but is supported by the material balance of the Au^{III} reduction in γ-radiolysis, which is over in less than 5 min after the end of irradiation. The upper limit of the first-order rate constant of this internal electron transfer/dissociation of the dimer $(Au^{II})_2$ into Au^{III} and Au^{I} can thus be estimated as $k_{21b} \leq 10^2$ s^{-1}. The spontaneous stabilization of the dimer $(Au^{II})_2$ compared to Au^{II} may be explained by the pairing of lone electrons. The monovalent gold ions Au^{I} eventually produced are very stable and hence accumulate. Indeed, Au^{I} ions are not reduced into Au_n by the radiolytic reducing species because all of them have been scavenged by Au^{III} after the pulse. Moreover, as pointed above, they do not undergo spontaneous disproportionation.

Note that, in water,[9] the decays of Au^{II} at 270 and 320 nm were assigned to a direct disproportionation reaction 21, but that some discrepancy has been found between the calculated values of $k_{12,water}$ at 270 and 320 nm. The rate constant of the process observed at 270 nm also depended on the Cl^- concentration and was comprised between 2.5×10^7 and 1.4×10^9 M^{-1} s^{-1}, so that a possible occurrence of an intermediate complexation process was evoked.[9]

It is also worthy to note that the dimerization of an unstable valency of a metal was already found in some examples other than Au^{II}. Indeed, the monovalent palladium ions Pd^{I} produced by pulse radiolysis in water do not disproportionate but first dimerize into $(Pd^{I})_2$.[37] No colloid formation was observed up to a few seconds after the pulse. Likewise, the transient pentavalent uranium ions are known to dimerize into $(U^{V})_2$.[38]

The absorption spectra of Au^{III}, Au^{II}, $(Au^{II})_2$, and Au^{I}, with their respective molar absorption coefficients, as obtained in Figure 1 via eqs 20 and eq 22 and in Figure 2 at 1.7 kJ L^{-1}, respectively (SI), are compared in Figure 7 in the range 250−625 nm. That of Au^{I} exhibits a very low, almost negligible, intensity. Except the additional band around 480 nm for Au^{II} and $(Au^{II})_2$, they all absorb more or less intensively in the same regions of 260 and 320 nm, and only an accurate analysis of the dose-dependent differential spectra enabled us to distinguish between them.

The scheme of Figure 8 summarizes the relative order of the reduction potential values of the various gold species formed in the solution compared to the potentials of the radiolytic species. The absolute values are unknown in 2-propanol, but we postulate that the order is the same as in water.[10] The mechanism of Au^{III} reduction is also illustrated (Figure 8), including some new processes demonstrated by this study. Namely, the formation of the dimer $(Au^{II})_2$, after the reduction of Au^{III} into Au^{II} by e_{solv}^- and $(CH_3)_2C^{\bullet}OH$, was inferred from the pulse radiolysis observations (Figures 3 and 5). From the γ-radiolysis results and the determination of the yields at each step (Figures 2), the induction period before the formation of

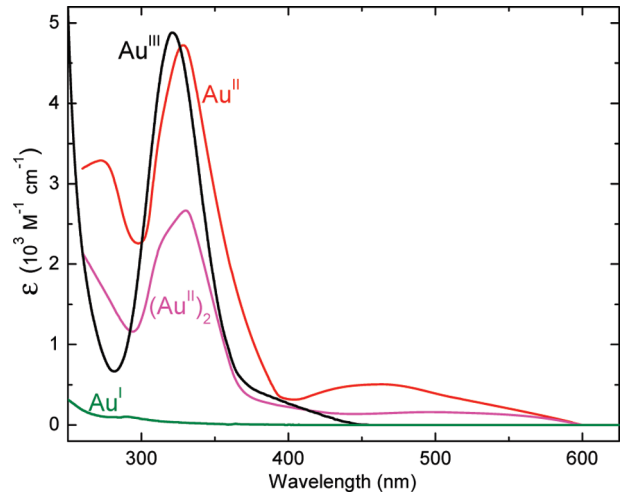

Figure 7. Comparison of optical absorption spectra in 2-propanol (in molar absorption coefficient) of Au^{III}, of Au^{I} ions as obtained from γ-radiolysis, and of transient Au^{II} and $(Au^{II})_2$ spectra as calculated from pulse radiolysis data.

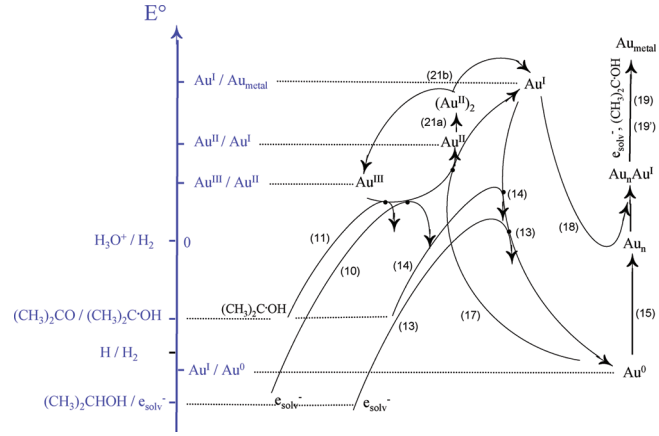

Figure 8. (Left) Scheme of reduction potentials of radiolytic reducing species compared with the potentials of gold ions in various valency states, ordered as in water. (Right) Mechanism of the homogeneous radiolytic reduction of Au^{III} in 2-propanol. The various reaction paths are inferred from direct observation by pulse radiolysis or from the yields measured by γ-radiolysis beyond and during the induction period for gold clusters appearance (see text).

gold clusters is accounted for by the internal electron transfer/dissociation of the dimer $(Au^{II})_2$ into Au^{III} and Au^{I}, and by the comproportionation of Au^0 with Au^{III} into Au^{II} and Au^{I}. Figure 8 illustrates how the very negative potential of the couple Au^{I}/Au^0 constitutes indeed a thermodynamical barrier to the reduction into Au_n. After the complete reduction of Au^{III} into Au^{I} by γ-radiolysis, only half of the alcohol radicals contribute to the clusters formation, possibly because the reactions between radicals are of comparable rates and compete.

Conclusion

Using the methodology of radiation chemistry (progressive dose-dependent reduction) and pulse radiolysis (time-resolved experiments), new processes have been evidenced in the reduction of trivalent gold ions that have been yet overlooked. They would occur also, whatever the reducing route used, similarly as in the radiolytic method.

The main contribution of the present work is to propose a coherent multistep reduction mechanism of Au^{III} ions into Au_n clusters. In particular, the feature of the linear decrease of Au^{III}

concentration at increasing dose until the complete reduction of Au^{III} and the induction dose before the cluster appearance, which is observed in 2-propanol and various other solvents including water, is explained by the strong reducing properties of gold atoms. More generally, the very negative reduction potential of metal atoms and their comproportionation with not yet reduced multivalent ions can explain similar results of the literature for other metals. The total reduction yield in 2-propanol obtained from methyl-viologen reduction by pulse radiolysis and from Au^{III} reduction into Au^{I} by γ-radiolysis is $G_{red} = 6 \times 10^{-7}$ mol J^{-1}. It was also shown that the divalent gold ions Au^{II} do not directly disproportionate, but dimerize into a long-lived dimer that then dissociates into Au^{III} and Au^{I}. Despite an overlapping in the same domain of the optical absorption spectra of all the transient species involved in the successive reactions, the different optical spectra and molar absorption coefficients have been established. The rate constants of the reduction of Au^{III} by alcohol radicals, of the dimerization of Au^{II} into the dimer $(Au^{II})_2$, followed by a slow internal electron transfer/dissociation of $(Au^{II})_2$ into Au^{I} and Au^{III} were evaluated.

Acknowledgment. The authors are indebted to Région Ile-de-France and to the French Ministry of Foreign Affairs for their financial support through the Indo-French ARCUS cooperation program. G.R.D is thankful to BARC-DAE India Authority for favoring him to interact with LCP researchers and is indebted to LINAC maintenance team for their support during pulse radiolysis experiments.

Supporting Information Available: Table 1: Wavelength-dependent molar optical absorption coefficients ε (in M^{-1} cm^{-1}) of Au^{III}, Au^{II}, $(Au^{II})_2$, and Au^{I} in 2-propanol. This material is available free of charge via the Internet at http://pubs.acs.org.

References and Notes

(1) Ferrando, R.; Jellinek, J.; Johnston, R. L. Nanoalloys: From theory to applications of alloy clusters and nanoparticles. *Chem. Rev.* **2008**, *108*, 845.

(2) Baxendale, J. H.; Busi, F. The study of fast processes and transient species by electron pulse radiolysis. *NATO ASI Series*; D. Reidel: Dordrecht, Holland, Boston, 1982.

(3) Belloni, J.; Mostafavi, M.; Remita, H.; Marignier, J.-L.; Delcourt, M.-O. *New J. Chem.* **1998**, *22*, 1239.

(4) Belloni, J.; Mostafavi, M. In *Studies in physical and theoretical chemistry: present status and future trends*; Jonah, C. D.; Rao, M., Eds.; Elsevier, New York, 2001; p 411.

(5) Buxton, G. V.; Mulazzani, Q. G.; Ross, A. B. *J. Phys. Chem. Ref. Data* **1995**, *24*, 1055. Ghosh-Mazumdar, A. S.; Hart, E. J. *Adv. Chem. Ser.* **1968**, *81*, 193–209.

(6) François, L.; Mostafavi, M.; Belloni, J.; Delaire, J. *Phys. Chem. Chem. Phys.* **2001**, *3*, 4965.

(7) Belloni, J. *Catal. Today* **2006**, *113*, 141.

(8) (a) Huang, X. H.; El-Sayed, I. H.; Qian, W.; El-Sayed, M. A. *J. Am. Chem. Soc.* **2006**, *128*, 2115. (b) Wu, X.; Ming, T.; Wang, X.; Wang, P.; Wang, J.; Chen, J. *ACS Nano* **2010**, *4*, 113.

(9) Baxendale, J. H.; Koulkes-Pujo, A.-M. *J. Chim. Phys.* **1970**, 1602.

(10) Gachard, E.; Remita, H.; Khatouri, J.; Keita, B.; Nadjo, L.; Belloni, J. *New J. Chem.* **1998**, *22*, 1257.

(11) Dey, G. R.; Kishore, K. *Radiat. Phys. Chem.* **2005**, *72*, 565.

(12) Dey, G. R. *Radiat. Phys. Chem.* **2005**, *74*, 172.

(13) Dey, G. R.; Remita, H.; Mostafavi, M. *Chem. Phys. Lett.* **2006**, *341*, 83.

(14) Guha, S. N.; Moorthy, P. N.; Kishore, K.; Naik, D. B.; Rao, K. N. *Proc. Indian Acad. Sci., Chem. Sci.* **1987**, *99*, 261.

(15) Buxton, G. V.; Stuart, C. R. *J. Chem. Soc., Faraday Trans.* **1995**, *91*, 279.

(16) Weast, R. C. *CRC Handbook in Chemistry and Physics*, 65th ed.; CRC Press: Boca Raton, FL, 1984−1985, D-155.

(17) Mostafavi, M.; Dey, G. R.; François, L.; Belloni, J. *J. Phys. Chem.* **2002**, *106*, 10184.

(18) Baxendale, J. H.; Wardman, P. *J. Chem. Soc., Faraday Trans. I* **1973**, *69*, 584.

(19) Getoff, N.; Ritter, A.; Schworer, F. P.; Bayer, *Radiat. Phys. Chem.* **1993**, *41*, 797.

(20) Afanasiev, A.; Kalyazin, E. P. In *Radiation Chemistry*; Dobo, J., Hedwig, P., Eds.; Akademiai Kiado: Budapest, 1972; p 71.

(21) (a) Simic, M.; Neta, P.; Hayon, E. *J. Phys. Chem.* **1969**, *73*, 3794. (b) Fowles, P. *Trans. Faraday Soc.* **1971**, *67*, 428. (c) Janata, E. *Proc. Indian Acad. Sci., Chem. Sci.* **2002**, *114*, 731.

(22) Buxton, G. V.; Greenstock, C. L.; Helman; Ross, A. B. *J. Phys. Chem. Ref. Data* **1988**, *17*, 513.

(23) Dorfman, L.; You, F. Y. In *Electrons in Fluids*; Jotrner, J., Kestner, N. R., Eds.; Springer: New York, 1973; p 447.

(24) Schwarz, H. A.; Dodson, R. W. *J. Phys. Chem.* **1989**, *93*, 409.

(25) Tausch-Treml, R.; Lilie, J.; Henglein, A. *Ber. Phys. Chem.* **1978**, *82*, 1335.

(26) Texier, I.; Mostafavi, M. *Radiat. Phys. Chem.* **1997**, *49*, 459.

(27) Anbar, M.; Hart, E. J. *Adv. Chem. Ser.* **1968**, *81*, 79. Mosseri, S.; Henglein, A.; Janata, E. *J. Phys. Chem.* **1989**, *93*, 6791.

(28) Treguer, M.; de Cointet, Ch.; Remita, H.; Khatouri, J.; Mostafavi, M.; Amblard, J.; Belloni, J.; De Keyzer, R. *J. Phys. Chem.* **1998**, *102*, 4310.

(29) Lide, D. R., Ed. In *Handbook of Chemistry and Physics*, 75th ed.; CRC Press: Boca Raton, FL, 1994; 5-5.

(30) Abidi, W.; Selvakannan, P. R.; Guillet, Y.; Lampre, I.; Beaunier, P.; Pansu, B.; Palpant, B.; Remita, H. *J. Phys. Chem. C* **2010**, *114*, 14794.

(31) Mirdamadi-Esfahani, M.; Mostafavi, M.; Keita, B.; Nadjo, L.; Kooyman, P.; Etcheberry, A.; Imperor, M.; Remita, H. *Gold Bull.* **2008**, *41*, 98.

(32) Henglein, A. *Chem. Rev.* **1989**, *89*, 1861.

(33) Sauer, M. C., Jr.; Arai, S.; Dorfman, L. *J. Chem. Phys.* **1965**, *42*, 708.

(34) Jay-Gerin, J. P.; Ferradini, C. *J. Chim. Phys.* **1994**, *91*, 173.

(35) Everett, S. A.; Folkes, L. K.; Wardman, P.; Asmus, K.-D. *Free Radical Res.* **1994**, *20*, 387.

(36) Watanabe, T.; Honda, K. *J. Phys. Chem.* **1982**, *86*, 2617.

(37) Michaelis, M.; Henglein, A. *J. Phys. Chem.* **1992**, *96*, 4719.

(38) Atinault, E.; De Waele, V.; Belloni, J.; Le Naour, C.; Fattahi, M.; Mostafavi, M. *J. Phys. Chem. A* **2010**, *114*, 2080.

JP1096597